

# Lawrence Berkeley National Laboratory

## LBL Publications

### Title

Ultrathin IBAD MgO films for epitaxial growth on amorphous substrates and sub-50 nm membranes

### Permalink

<https://escholarship.org/uc/item/5jj6n0b1>

### Journal

Applied Physics Letters, 109(19)

### ISSN

0003-6951

### Authors

Wang, Siming  
Antonakos, C.  
Bordel, C.  
[et al.](#)

### Publication Date

2016-11-09

## Ultrathin IBAD MgO films for epitaxial growth on amorphous substrates and sub-50 nm membranes

Siming Wang,<sup>1,2,a)</sup> C. Antonakos,<sup>3,a)</sup> C. Bordel,<sup>1,2,4</sup> D. S. Bouma,<sup>1,2</sup> P. Fischer,<sup>1,5</sup> and F. Hellman<sup>1,2,b)</sup>

<sup>1</sup>Materials Sciences Division, Lawrence Berkeley National Laboratory, Berkeley, California 94720, USA

<sup>2</sup>Department of Physics, University of California Berkeley, Berkeley, California 94720, USA

<sup>3</sup>Department of Chemistry, University of California Berkeley, Berkeley, California 94720, USA

<sup>4</sup>GPM, UMR 6634 CNRS-Université de Rouen, 76801 St. Etienne du Rouvray, France

<sup>5</sup>Department of Physics, University of California Santa Cruz, Santa Cruz, California 94056, USA

(Received 24 August 2016; accepted 16 October 2016; published online 9 November 2016)

A fabrication process has been developed for high energy ion beam assisted deposition (IBAD) biaxial texturing of ultrathin ( $\sim 1$  nm) MgO films, using a high ion-to-atom ratio and post-deposition annealing instead of a homoepitaxial MgO layer. These films serve as the seed layer for epitaxial growth of materials on amorphous substrates such as electron/X-ray transparent membranes or nanocalorimetry devices. Stress measurements and atomic force microscopy of the MgO films reveal decreased stress and surface roughness, while X-ray diffraction of epitaxial overlayers demonstrates the improved crystal quality of films grown epitaxially on IBAD MgO. The process simplifies the synthesis of IBAD MgO, fundamentally solves the “wrinkle” issue induced by the homoepitaxial layer on sub-50 nm membranes, and enables studies of epitaxial materials in electron/X-ray transmission and nanocalorimetry. *Published by AIP Publishing.*

[<http://dx.doi.org/10.1063/1.4966956>]

Developing techniques for the integration of amorphous and epitaxial thin films is crucial for basic materials research and technological applications.<sup>1</sup> Advanced structural characterization by X-ray and electron transmission demands a film including its substrate, typically a thin amorphous silicon nitride ( $a$ -SiN<sub>x</sub>) membrane, that is transparent to X-ray<sup>2</sup> and electron beams.<sup>3</sup> Thermodynamics studies of thin film materials require films to be deposited on suspended membranes of  $a$ -SiN<sub>x</sub> which provide thermal isolation.<sup>4,5</sup> Many thin films of scientific and technological interest are however best grown as epitaxial materials. One approach to resolve this challenge is to deposit a biaxially textured “seed” layer through ion beam assisted deposition (IBAD), which in turn enables relatively high-crystalline-quality epitaxial growth of the desired material.<sup>1,6–14</sup> In IBAD growth, as MgO is deposited on the amorphous substrate, it is simultaneously etched by high energy (600–1000 eV) Ar<sup>+</sup> ions at a 45° incident angle. After 2–10 nm IBAD MgO deposition, both out-of-plane (001) and in-plane texturing ((101) parallel to the 45° ion beam) form in the MgO layer, due to preferential removal of MgO of other orientations.<sup>1,12–14</sup> In the “standard” method used for high energy IBAD MgO biaxial texturing, a subsequent homoepitaxial MgO layer (made without the ion beam) is grown, enabling the growth of an epitaxial film of some other material.<sup>1,12,14</sup> This technique enabled, e.g., calorimetry studies of epitaxial FeRh films.<sup>15,16</sup> Alternatively, a thick (10 nm) IBAD MgO with post-deposition annealing yielded promising results.<sup>17</sup>

However, two fundamental challenges remain unresolved. First, these processes induce a substantial stress in

the MgO and the underlying substrate,<sup>4,18</sup> which is visible as wrinkling of the 30 nm membrane of a nanocalorimetry device.<sup>18</sup> Second, the 10–15 nm MgO thickness (in addition to the sample itself) is thicker than optimal for many transmission studies. In this paper, we demonstrate a process for preparing epitaxial films on an amorphous substrate, using post-deposition annealing of ultrathin IBAD MgO films ( $\sim 1$  nm) with no homoepitaxial MgO layer. This process is enabled by a high ion-to-atom ratio (IAR) in the IBAD process which enables the development of strong biaxial texturing by  $\sim 1$  nm film thickness. This process significantly simplifies the fabrication of the IBAD MgO, reduces its thickness, stress, and surface roughness, eliminating the visible “wrinkles” of the sub-50 nm membrane shown in Ref. 18, and improves the quality of the subsequent epitaxial film.

IBAD MgO thin films were deposited at room temperature onto thermal  $a$ -SiO<sub>x</sub> or  $a$ -SiN<sub>x</sub> (deposited by low pressure chemical vapour deposition on Si (001) substrates or as membranes) in high vacuum (base pressure  $2 \times 10^{-8}$  Torr; pressure during IBAD growth  $1 \times 10^{-4}$  Torr Ar). MgO was evaporated by an electron beam gun at a rate of 1.12 Å/s. During IBAD deposition, the growing film of textured (001) MgO was bombarded with 750 eV Ar<sup>+</sup> ions at a 45° incident angle, causing biaxial texturing in the IBAD MgO. The beam current was measured to be 10 mA, yielding an IAR of 1.98 (see the definition of IAR in the [supplementary material](#)), and an accumulation rate of the IBAD MgO on the substrate of 0.15 Å/s (characterized by X-ray reflectivity of a several nm thick film). 45–60 s of growth gives  $\sim 1$  nm IBAD MgO thickness. This IAR is of order ten times higher than that usually used,<sup>4</sup> and results in approximately 90% of the MgO being removed as it is deposited. The substrate temperature typically increases from room temperature by 10–15 °C due to Ar<sup>+</sup>

<sup>a)</sup>S. Wang and C. Antonakos contributed equally to this work.

<sup>b)</sup>Author to whom correspondence should be addressed. Electronic mail: fhellman@lbl.gov

bombardment and/or MgO growth. “Standard” high energy IBAD MgO biaxial texturing, used for example, in Ref. 4, was also prepared in which the IBAD MgO layer is followed *in situ* by a 10–15 nm homoepitaxial MgO layer grown at a rate of 0.08 Å/s at 350 °C (pressure  $\sim 2 \times 10^{-8}$  Torr as the Ar gas is pumped away) which improves the quality of the MgO film (and the epitaxial quality of subsequent films). *In situ* reflection high energy electron diffraction (RHEED) is performed during both IBAD and homoepitaxial MgO deposition to verify biaxially textured/epitaxial growth, respectively.<sup>19</sup>

In the present work, we studied both the “standard” IBAD MgO (IBAD layer + homoepitaxial MgO layer) and ultrathin IBAD-only MgO, each grown and annealed at various temperatures. 100 nm Fe films were then deposited onto these various types of IBAD MgO as well as onto single-crystalline MgO (001) substrates for control substrates to examine the quality of epitaxy enabled by IBAD MgO. Fe was evaporated by an electron beam gun at a rate of 0.48–0.52 Å/s with the substrate temperature at 200 °C.

The first and most notable result is that biaxially textured IBAD MgO films are seen in RHEED after only  $\sim 1$  nm has been grown (Fig. 1(b) in [supplementary material](#)),<sup>19</sup> thinner than the usual critical thickness up to which polycrystallinity is observed.<sup>1,14</sup> Due to the high IAR here used, approximately 90% of the MgO molecules arriving at the substrate are etched away, enabling a high degree of preferential growth of the in-plane textured grains ([101] parallel to the ion beam). These films are rough and under compressive stress, but annealing eliminates these effects, as will be discussed below, leaving annealed  $\sim 1$  nm IBAD MgO as a high quality platform for epitaxial growth of other films.

Growth of IBAD with or without subsequent homoepitaxial MgO films creates stress in the films and substrates, which can be reduced by annealing. We study the as-grown stress and the effect of annealing at temperatures from 500–800 °C by measuring the radius of curvature of the wafer (Eq. (1) in [supplementary material](#)). Three different IBAD MgO samples were measured: IBAD-only MgO, IBAD + 5 nm homoepitaxial MgO grown at 350 °C, and IBAD + 15 nm homoepitaxial MgO grown at 350 °C. These samples were grown on 2 in. Si (001) wafers with 100 nm of thermal  $\alpha$ -SiO<sub>x</sub>. Before any MgO growth, all wafers were annealed under vacuum at 800 °C for 30 min, then the radius of curvature measured, so that changes in wafer curvature after post-growth anneals can be attributed to change of the MgO film stress rather than annealing-induced change in the thermal oxide or Si wafer. Each sample was measured as grown and after each 30 min annealing step, and all measurements were taken at room temperature. Previous synchrotron X-ray diffraction (XRD) measurements showed asymmetry (relative to the Ar<sup>+</sup> ion beam direction) in the in-plane lattice constants of IBAD MgO.<sup>4</sup> Therefore, the wafer curvature was measured both parallel (Fig. 1(a)) and perpendicular (Fig. 1(b)) to the in-plane projection of the Ar<sup>+</sup> ion beam.

Figure 1 shows the stress of as-grown IBAD MgO-only is compressive, with a value for the direction perpendicular to the ion beam approximately twice that parallel to the ion beam. The relatively large as-grown compressive stress of the IBAD-only MgO film decreases drastically upon annealing at 500 °C, resulting in a slightly tensile film. The two

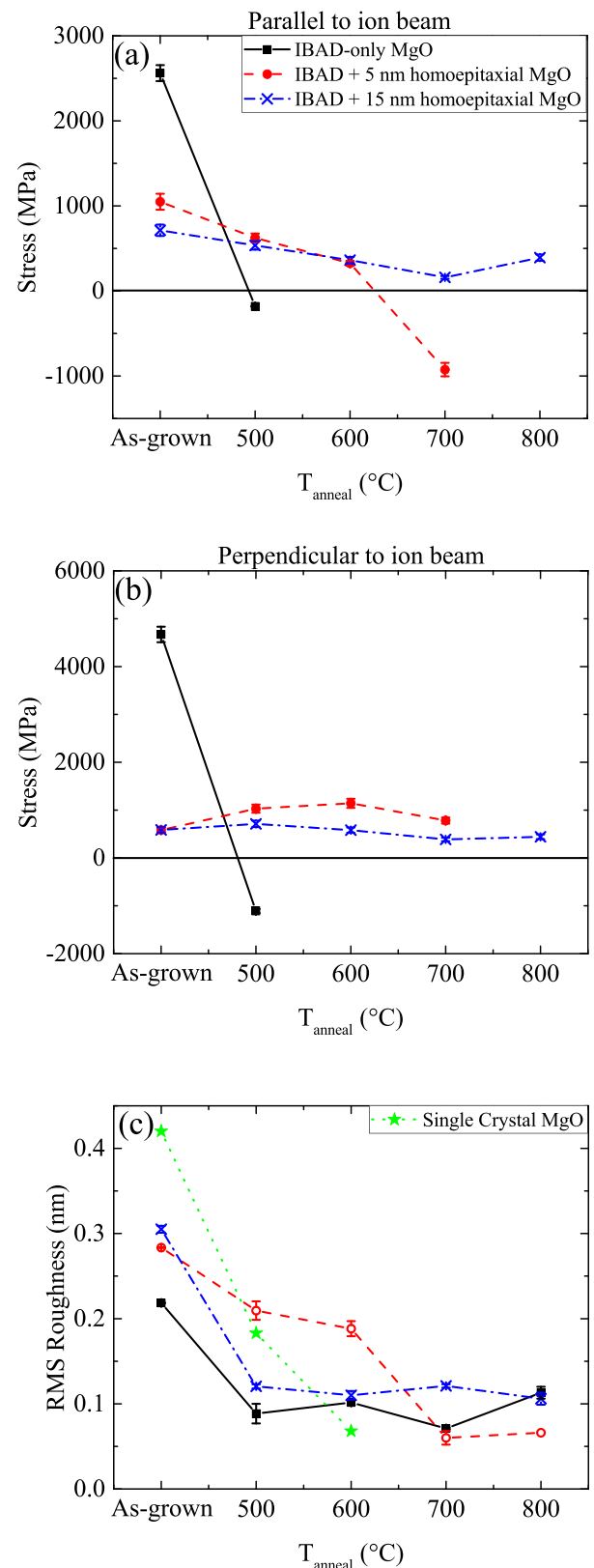


FIG. 1. Stress of IBAD MgO films ( $>0$  for compressive and  $<0$  for tensile) measured by radius of wafer curvature as grown and after annealing: (a) and (b) parallel and perpendicular to the in-plane projection of the ion beam during IBAD MgO growth. (c) RMS roughness of IBAD MgO films and single crystal MgO (001) substrates measured by AFM as grown and after annealing. Each plot shows three different IBAD MgO: IBAD-only MgO, IBAD + 5 nm homoepitaxial MgO grown at 350 °C, and IBAD + 15 nm homoepitaxial MgO grown at 350 °C. Error bars for stress are calculated with standard errors from substrate thickness, film thickness, and radius of curvature; error bars for roughness are the standard errors from two AFM measurements taken at different locations on the sample.

IBAD + homoepitaxial MgO films are also compressive as grown, with some in-plane asymmetry, and show a more gradual decrease with annealing; annealing at 800 °C still does not fully relax the stress. Comparing the different films in their as-grown states, the stress in the as-grown IBAD + homoepitaxial MgO films is lower than that in the as-grown IBAD-only MgO film, and that in the 15 nm homoepitaxial layer lower than for the 5 nm homoepitaxial layer. These differences could be due to annealing of the IBAD MgO underlayer during the slow deposition of the homoepitaxial layer at 350 °C (10–30 min for 5–15 nm homoepitaxial MgO). Alternatively, an increased stress from the initial stages of homoepitaxial layer could cause dislocations to form and propagate through the film, which relaxes the stress.

We also investigated the effect of IBAD and homoepitaxial MgO growth on *a*-SiN<sub>x</sub> membranes, which are used, e.g., for calorimetry. Previous work showed that thin membranes (30 nm thick) are sufficiently stressed as to become visibly wrinkled, making them unsuitable as epitaxial sample platforms.<sup>18</sup> In this work, we study 30 nm thick *a*-SiN<sub>x</sub> membranes, identical to those used for nanocalorimetry devices. The fabrication and use of these devices are described in Refs. 20 and 21. IBAD + homoepitaxial MgO depositions created visibly wrinkled membranes shown in Fig. 2(a), consistent with Ref. 18. Annealing at 500 °C reduced the stress, still however leaving visible wrinkles at the edges of Pt electrodes shown in Fig. 2(b). But, most significantly, as shown in Figs. 2(c) and 2(d), ultrathin IBAD-only MgO did not create any wrinkles, and annealing at 500 °C did not affect the membrane and the device, opening up the possibility of making thin epitaxial samples on sub-50 nm membranes. We note that the IBAD + homoepitaxial MgO film causes more wrinkles in the membrane even

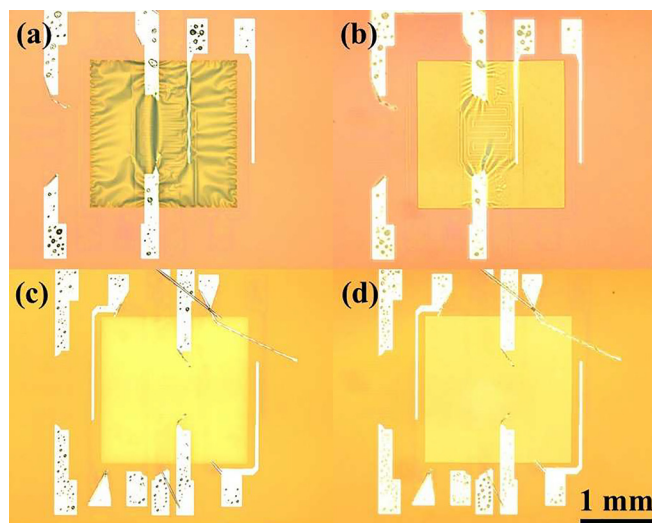


FIG. 2. Optical microscope images of nanocalorimeters, showing  $0.5 \times 0.5 \text{ cm}^2$  Si frame, with  $0.2 \times 0.2 \text{ cm}^2$  30 nm thick *a*-SiN<sub>x</sub> membrane at center; silver-colored pads show Pt electrical leads and contacts used in calorimetry (devices with damaged Pt were used for these experiments). (a) Nanocalorimeter after IBAD and 15 nm homoepitaxial MgO deposition and (b) after annealing at 500 °C for 30 min. Strain is clearly visible (wrinkles) in (a), and is partly relieved in (b) after annealing. (c) Nanocalorimeter after 1 nm IBAD MgO deposition (without homoepitaxial layer) and (d) after annealing at 500 °C for 30 min. No strain is visible either as grown or after annealing.

though the stress is lower than IBAD-only MgO (data in Figs. 1(a) and 1(b)); this effect is simply due to the different thicknesses of both the film and the substrate. The deformation (or wrinkles) in the membrane is equivalent to the curvature change  $\Delta R = \Delta R_{film} - \Delta R_{no\ film}$ , which (see Eq. (1) in [supplementary material](#)) is proportional to the product of stress and film thickness  $\sigma * t$ . This product for the IBAD + homoepitaxial MgO film is approximately four times higher than for IBAD-only MgO film, leading to higher  $\Delta R$ ; i.e., the stress shown in Figs. 1(a) and 1(b) is consistent with the visible changes shown in Fig. 2.

The surface flatness of MgO is important to its use as a seed layer for epitaxial films. In addition to intrinsic growth-induced roughness, high annealing temperatures could potentially destabilize the (001) MgO surface and increase its surface roughness. We used atomic force microscopy (AFM) to study the roughness of various IBAD MgO films and single crystal (001) MgO substrates annealed at various temperatures from 500–800 °C. Three different IBAD MgO samples were measured using AFM: IBAD-only MgO, IBAD + 5 nm homoepitaxial MgO grown at 350 °C, and IBAD + 15 nm homoepitaxial MgO grown at 350 °C. These samples were grown on  $1 \text{ cm}^2$  Si (001) substrates with 100 nm of *a*-SiN<sub>x</sub>. Each sample was measured as-grown and after each 30 min annealing step, and all measurements were taken at room temperature.

Figure 1(c) shows the as-grown and post-annealing rms roughness of the three MgO films and a single crystal MgO. For the as-grown films, the roughness of the IBAD-only MgO is  $\sim 0.2 \text{ nm}$ , lower than that of the IBAD + homoepitaxial MgO which is  $\sim 0.3 \text{ nm}$ . Annealing at 500–800 °C reduced the surface roughness to  $\sim 0.1 \text{ nm}$  for all samples, including the single crystal MgO. Annealing at 500 °C is sufficient to minimize the surface roughness of IBAD-only MgO. No clear change in surface roughness is observed for annealing at 800 °C, suggesting that the epitaxial growth is possible at this high temperature. Interestingly, the annealing significantly reduced the rms roughness of the single crystal MgO (001); 100s of nm stripes were observed on the surface of the pristine epi-polished MgO in AFM, which were removed after annealing at 600 °C. MgO (001) has lower surface energy than (110) and (111) according to a previous thermal faceting study,<sup>22</sup> which explains the reduction of surface roughness by annealing observed here. The effect of annealing was studied previously for thick MgO films (e.g., 120 nm in Ref. 23), but the rms roughness was higher in those thick as-grown films (2–4 nm), and was unchanged after annealing.

AFM images of as-deposited IBAD-only MgO and IBAD + 15 nm homoepitaxial MgO show similar surface cubic nanostructures with  $\sim 50 \text{ nm}$  lateral size. Annealing significantly reduces this structure and smooths the film surface for both films (cubic structure essentially eliminated, consistent with reduced rms roughness shown in Fig. 1) (AFM images shown in Fig. 2s(a)–2s(d) of [supplementary materials](#)).

We further study the quality of IBAD-only and IBAD + homoepitaxial MgO layers under various annealing conditions by using X-ray diffraction (XRD) to characterize the epitaxy of Fe films grown on these “substrates” compared to those grown on single crystal MgO substrates (also either

annealed or not). The low thickness (between 1 nm and 16 nm) and low scattering factor of MgO preclude measuring XRD peaks with our diffractometer, but it is the quality of the epitaxial layer grown on the MgO that matters in a calorimetry or an X-ray microscopy experiment. We investigated 100 nm Fe layers grown at 200 °C on seven different MgO “substrates.”

Out-of-plane  $2\theta/\omega$  scans of all samples show the Fe (002) peak, suggesting epitaxial growth of Fe. Figure 3(a) shows the intensity near the (002) peak, evidencing a similar Fe lattice constant for all. A peak just above the noise level is observed at 44.7° for IBAD + 15 nm homoepitaxial MgO grown at 350 °C, which corresponds to the Fe (110) orientation, suggesting a small fraction of polycrystalline Fe on the homoepitaxial MgO. Figure 3(b) shows the  $\phi$  scans of Fe on the same substrates, with the  $2\theta$  and  $\psi$  angles aligned to Fe (101). Strong peaks are observed at 45° and 135°, indicating four-fold in-plane symmetry of the Fe, enabled by the IBAD MgO biaxial (in-plane and out-of-plane) texturing.

Overall, Fe films on single crystal MgO substrates show better crystal quality (lower FWHM of  $\omega$ ,  $2\theta$ , and  $\phi$ , shown in Figs. 3s(a), 3s(b), and 3s(d) of [supplementary material](#)) and significantly higher intensity than those on any IBAD

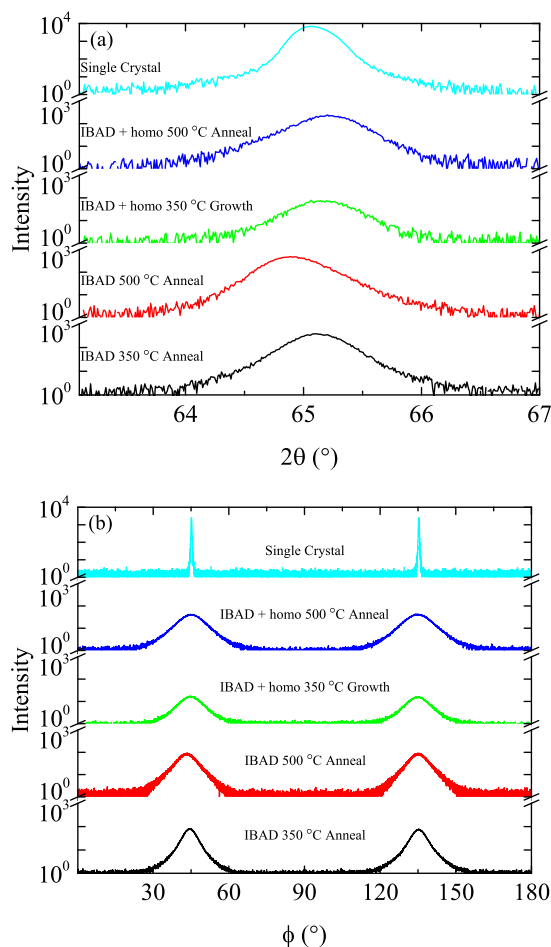


FIG. 3. (a) Out-of-plane  $2\theta/\omega$  scan and (b)  $\phi$  scan of 100 nm Fe film grown at 200 °C on: IBAD-only MgO annealed at 350 °C (black), IBAD-only MgO annealed at 500 °C (red), IBAD + 15 nm homoepitaxial MgO as grown at 350 °C (green), IBAD + 15 nm homoepitaxial MgO annealed at 500 °C (blue), and single crystal MgO (001) (cyan). Note that the XRD intensity (in counts per second) is normalized by the baseline (in counts per second), resulting in a dimensionless normalized intensity.

MgO, but Fe on IBAD-only MgO *without* the homoepitaxial layer ( $<1.6^\circ$  FWHM of  $\omega$  and  $<8^\circ$  FWHM of  $\phi$ ) has better crystal quality than Fe on IBAD MgO *with* homoepitaxial layer ( $>2.2^\circ$  FWHM of  $\omega$  and  $>9^\circ$  FWHM of  $\phi$ ). XRD of similar IBAD + homoepitaxial MgO shows  $\sim 3^\circ$  FWHM of  $\omega$  and  $\sim 7^\circ$  FWHM of  $\phi$ ,<sup>12,17</sup> comparable to the values shown in Figs. 3s(a) and 3s(d) of [supplementary material](#). For thicker homoepitaxial layers ( $>100$  nm), the FWHM of  $\omega$  ( $1^\circ$ – $2^\circ$ ) and  $\phi$  ( $3^\circ$ – $5^\circ$ ) are lower; and the FWHM decreases with increasing homoepitaxial layer thickness.<sup>24</sup> However, such a thick homoepitaxial layer is not desired for transmission X-ray/electron microscopy or nanocalorimetry studies.

We compare the epitaxy of Fe on post-annealed IBAD-only MgO samples with that from other epitaxial/texturing deposition techniques: (1) pulsed laser deposition of 20 nm MgO (001) on Si (001);<sup>25</sup> (2) 11 nm IBAD + 100 nm homoepitaxial MgO (001) on a flexible ceramic;<sup>26</sup> (3) domain matching epitaxy of 20–80 nm MgO (001) on Si (001);<sup>27</sup> (4) energetic particle self-assist deposition of 10 nm biaxially textured MgO (111) on amorphous surfaces.<sup>28</sup> The FWHM of  $\omega$  and  $\phi$  scans from Fe on IBAD-only MgO are lower than that from the MgO reported in the above literature, further demonstrating the quality of our IBAD-only MgO.

The (002) peak of Fe on IBAD-only MgO annealed at 500 °C also has the highest integrated intensity among the IBAD samples (shown in Fig. 3s(c) of [supplementary material](#)), meaning the highest volume of epitaxial Fe, consistent with previous studies in which the out-of-plane peak from the annealed MgO was directly measured.<sup>23,29,30</sup> The lowest FWHM and highest integrated intensity of the (002) peaks of Fe for the IBAD-only MgO annealed at 500 °C suggest that this annealing temperature renders the best surface for epitaxial growth among the four IBAD MgO samples shown in Fig. 3. The coherence length of the Fe layers is estimated with Scherrer equation (Eq. (2) of [supplementary material](#)). The out-of-plane coherence length ( $\sim 20$  nm) is smaller than the film thickness ( $\sim 100$  nm); the in-plane coherence length ( $\sim 10$  nm) is smaller than the grain size of the IBAD MgO ( $\sim 50$  nm). This result suggests defects such as low angle grain boundaries in the Fe, which may explain small shifts seen in the Fe (002)  $2\theta$  peak.

In summary, we developed a process to fabricate ultrathin ( $\sim 1$  nm) IBAD MgO films through high ion-atom-ratio growth followed by post-deposition annealing, yielding a high quality seed layer for epitaxial film growth. The 500 °C annealed ultrathin IBAD MgO film has very low stress and surface roughness, and yields a higher quality epitaxial Fe growth, thus offering a replacement to the “standard” thick IBAD + homoepitaxial layer previously used. Most notably, the ultrathin IBAD MgO enables the growth of epitaxial films on thin amorphous membranes (under 50 nm) useful to nanocalorimetry and *in situ* heater stages for transmission electron or X-ray microscopy, *without* producing visible wrinkles in the membrane that impede structural characterization. This process simplifies the IBAD MgO synthesis and provides a simpler means of producing epitaxial films on amorphous membrane substrates, with broad application potential in fundamental materials research and industrial fabrication processes.

See [supplementary material](#) for experimental methods for RHEED, stress measurement, AFM and XRD; the definition of IAR; RHEED images before and after IBAD MgO deposition; AFM images of IBAD MgO films; FWHM of  $\omega$ , integrated intensity of  $2\theta$  peaks, and FWHM of  $\phi$  for Fe on IBAD and single crystal MgO.

This work was supported by the Director, Office of Science, Office of Basic Energy Sciences, Materials Sciences and Engineering Division, of the U.S. Department of Energy under Contract No. DE-AC02-05-CH11231 within the Nonequilibrium Magnetic Materials Program (KC2204). C.A. acknowledges the support from an NSF Graduate Fellowship.

- <sup>1</sup>V. Matias and R. H. Hammond, *Surf. Coat. Technol.* **264**, 1 (2015).
- <sup>2</sup>P. Fischer, D.-H. Kim, W. Chao, J. A. Liddle, E. H. Anderson, and D. T. Attwood, *Mater. Today* **9**, 26 (2006).
- <sup>3</sup>M. C. Scott, C.-C. Chen, M. Mecklenburg, C. Zhu, R. Xu, P. Ercius, U. Dahmen, B. C. Regan, and J. Miao, *Nature* **483**, 444 (2012).
- <sup>4</sup>D. W. Cooke, F. Hellman, J. R. Groves, B. M. Clemens, S. Moyerman, and E. E. Fullerton, *Rev. Sci. Instrum.* **82**, 023908 (2011).
- <sup>5</sup>D. W. Cooke, F. Hellman, C. Baldasseroni, C. Bordel, S. Moyerman, and E. E. Fullerton, *Phys. Rev. Lett.* **109**, 255901 (2012).
- <sup>6</sup>Y. Iijima, N. Tanabe, O. Kohno, and Y. Ikeno, *Appl. Phys. Lett.* **60**, 769 (1992).
- <sup>7</sup>M. J. Dicken, K. Diest, Y.-B. Park, and H. A. Atwater, *J. Cryst. Growth* **300**, 330 (2007).
- <sup>8</sup>A. T. Findikoglu, W. Choi, V. Matias, T. G. Holesinger, Q. X. Jia, and D. E. Peterson, *Adv. Mater.* **17**, 1527 (2005).
- <sup>9</sup>J. R. Groves, J. B. Li, B. M. Clemens, V. Lasalvia, F. Hasoon, H. M. Branz, and C. W. Teplin, *Energy Environ. Sci.* **5**, 6905 (2012).
- <sup>10</sup>P. Dutta, M. Rathi, N. Zheng, Y. Gao, Y. Yao, J. Martinez, P. Ahrenkiel, and V. Selvamanickam, *Appl. Phys. Lett.* **105**, 092104 (2014).
- <sup>11</sup>S. Cardoso, R. J. Macedo, R. Ferreira, A. Augusto, P. Wisniowski, and P. P. Freitas, *J. Appl. Phys.* **103**, 07A905 (2008).
- <sup>12</sup>C. P. Wang, K. B. Do, M. R. Beasley, T. H. Geballe, and R. H. Hammond, *Appl. Phys. Lett.* **71**, 2955 (1997).
- <sup>13</sup>R. T. Brewer and H. A. Atwater, *Appl. Phys. Lett.* **80**, 3388 (2002).
- <sup>14</sup>J. R. Groves, R. H. Hammond, V. Matias, R. F. DePaula, L. Stan, and B. M. Clemens, *Nucl. Instrum. Methods Phys. Res., Sect. B* **272**, 28 (2012).
- <sup>15</sup>A. X. Gray, D. W. Cooke, P. Krüger, C. Bordel, A. M. Kaiser, S. Moyerman, E. E. Fullerton, S. Ueda, Y. Yamashita, A. Gloskovskii, C. M. Schneider, W. Drube, K. Kobayashi, F. Hellman, and C. S. Fadley, *Phys. Rev. Lett.* **108**, 257208 (2012).
- <sup>16</sup>C. Baldasseroni, C. Bordel, C. Antonakos, A. Scholl, K. H. Stone, J. B. Kortright, and F. Hellman, *J. Phys.: Condens. Matter* **27**, 256001 (2015).
- <sup>17</sup>O. Polat, T. Aytug, M. Paranthaman, K. Kim, Y. Zhang, J. R. Thompson, D. K. Christen, X. Xiong, and V. Selvamanickam, *J. Mater. Res.* **23**, 3021 (2008).
- <sup>18</sup>D. W. Cooke, D. R. Queen, and F. Hellman, see <http://www.aps.org/meetings/march/vpr/2010/imagegallery/membrane.cfm> for Strain Fields of a Buckled Silicon Nitride Membrane (2010).
- <sup>19</sup>C. D. Antonakos, "I. Measuring and reducing stress and surface roughness in IBAD MgO films and II. Developing tools to measure transfer in undergraduate chemistry students," Ph.D. dissertation, University of California Berkeley, Berkeley CA, 2016.
- <sup>20</sup>D. W. Denlinger, E. N. Abarra, K. Allen, P. W. Rooney, M. T. Messer, S. K. Watson, and F. Hellman, *Rev. Sci. Instrum.* **65**, 946 (1994).
- <sup>21</sup>D. R. Queen and F. Hellman, *Rev. Sci. Instrum.* **80**, 063901 (2009).
- <sup>22</sup>V. E. Henrich, *Surf. Sci.* **57**, 385 (1976).
- <sup>23</sup>A. Vannozi, V. Galluzzi, A. Mancini, A. Rufolini, A. Augieri, A. Angrisani Armenio, L. Ciontea, Gy. Thalmaier, T. Petrisor, and G. Celentano, *IEEE Trans. Appl. Supercond.* **21**, 2908 (2011).
- <sup>24</sup>V. Matias, B. J. Gibbons, J. Hanisch, R. J. A. Steenwelle, P. Dowden, J. Rowley, J. Y. Coulter, and D. Peterson, *IEEE Trans. Appl. Supercond.* **17**, 3263 (2007).
- <sup>25</sup>C. Martínez Boubeta, A. Cebollada, J. F. Calleja, C. Contreras, F. Peiró, and A. Cornet, *J. Appl. Phys.* **93**, 2126 (2003).
- <sup>26</sup>R. Lu, J. Z. Wu, C. Varanasi, J. Burke, I. Maartense, and P. N. Barnes, *J. Electron. Mater.* **36**, 1258 (2007).
- <sup>27</sup>H. K. Yu and J.-L. Lee, *Cryst. Growth Des.* **10**, 5200 (2010).
- <sup>28</sup>S. Xiao, F. Feng, T. Qu, H. Lu, X. Zhang, and Z. Han, *IEEE Trans. Appl. Supercond.* **26**, 7500805 (2016).
- <sup>29</sup>A. Ide-Ekessabi, H. Nomura, N. Yasui, and Y. Tsukuda, *Surf. Coat. Technol.* **163–164**, 728 (2003).
- <sup>30</sup>Z. Yu, W. Xue, D. Zheng, and J. Sun, *Plasma Sci. Technol.* **9**, 284 (2007).